Journal of Inorganic and General Chemistry
ZAAC
Zeitschrift für anorganische und allgemeine Chemie
www.zaac.wiley-vch.de
RESEARCH ARTICLE
Check for updates
DOI: 10.1002/zaac.202400013

Reactions of Dichloroacetyl Fluoride in Superacidic Media

Sebastian Steiner,[a] Alexander Nitzer,[a] Christoph Jessen,[a] and Andreas J. Kornath*[a]

Dichloroacetyl fluoride was investigated in the superacids HF/MF_5 and DF/MF_5 (M = As, Sb). The *O*-hemiprotonated species of dichloroacetyl fluoride is formed in the binary superacidic systems HF/MF_5 and DF/MF_5 (M = As, Sb) as hexafluoridoarsenates and hexafluoridoantimonates. With an excess of the strong Lewis acid SbF_5 dichloroacetyl fluoride reacts under the formation of the oxonium salt $[CCl_2HCF_2OX_2][SbF_6]$ in the superacidic system XF/SbF_5 (X = H, D) after HF- or DF-addition, respectively. The colorless salts were characterized by low-temperature vibrational spectroscopy, NMR spectroscopy, and single-crystal X-ray diffraction. $[CCl_2HC(OH)F][(CCl_2HCOF)_2H][SbF_6][Sb_2F_{11}]$ and $[CCl_2HCF_2OH_2][SbF_6]$ crystallize in the monoclinic space groups $P2_1/c$ and $P2_1/m$, respectively, with two formula units per unit cell each. The crystal structure of the oxonium salt shows strong O(–H)···F hydrogen bonds and strong F···F interactions. The experimental data are discussed together with quantum chemical calculations at the ωB97XD/aug-cc-pVTZ-level of theory.

Introduction

Oxonium ions of the type $R\text{-}OH_2^+$ (R = alkyl) are formed by the protonation of alcohols in superacidic media. When ketones are reacted in superacidic media, HF-addition to the carbonyl groups occurs under the formation of an OH group, which is subsequently protonated.[1–4] In many cases, the protonation was observed, when the alkyl group is substituted with strongly electron-withdrawing atoms, such as perfluorinated alkyl moieties.[2–7] Minkwitz investigated hexafluoroacetone in the binary superacidic system HF/SbF_5 and characterized the tertiary oxonium salt $[(CF_3)_2C(F)OH_2][Sb_2F_{11}]$, which was formed by protonation of the intermediate α-fluoroalcohol.[2] The simplest case is COF_2, to which HF is added in the superacidic media forming CF_3OH that is subsequently protonated to $[CF_3OH_2][SbF_6]$.[3,4]

In previous studies of our group, monoprotonated species of chloroacetyl fluoride and fluoroacetyl fluoride were isolated and characterized, but no oxonium ions were observed.[8] Recently, we observed a protonation of the keto group in carbonyl fluorides by superacids for the first time in the case of fumaryl fluoride.[9] This prompted us to perform further investigations on simpler carbonyl fluorides. We report herein the reaction of dichloroacetyl fluoride in the superacidic system HF/MF_5 (M = As, Sb).

[a] S. Steiner, A. Nitzer, C. Jessen, A. J. Kornath
Department Chemie, Ludwig-Maximilians-Universität München, Butenandtstraße 5–13, 81377 Munich, Germany
E-mail: andreas.kornath@cup.uni-muenchen.de
Homepage: http://www.org.chemie.uni-muenchen.de/ac/kornath

Supporting information for this article is available on the WWW under https://doi.org/10.1002/zaac.202400013

Results and Discussion

Synthesis and Properties of $[(CCl_2HCOF)_2X][MF_6]$ and $[CCl_2HCF_2OX_2][SbF_6]$ (X = H, D; M = As, Sb)

At first, dichloroacetyl fluoride was reacted in the binary superacidic system XF/MF_5 (X = H, D; M = As, Sb). The Lewis acid and anhydrous hydrogen fluoride or deuterium fluoride, respectively, were condensed into a FEP tube reactor. To form the superacid, both components were mixed at −50 °C. After dichloroacetyl fluoride was condensed into the reaction vessel at −196 °C, the mixture was reacted at −60 °C for 15 min, and the remaining HF was removed in a dynamic vacuum. *O*-hemiprotonated species of dichloroacetyl fluoride were obtained according to Equation 1 as hexafluoridoarsenates (**1**, **3**) and hexafluoridoantimonates (**2**, **4**) in quantitative yields as colorless solids.

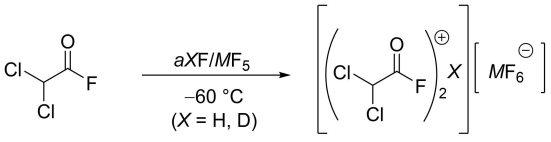

(1)

With the aim to obtain the fully monoprotonated species, dichloroacetyl fluoride was reacted in the binary superacidic systems HF/SbF_5 and DF/SbF_5 with a fourfold excess of the strong Lewisacid SbF_5. Instead of the desired species, the oxonium salts (**5a**) and (**6**) were formed as colorless solids after the addition of HF or DF, respectively, as presented in Equation 2.

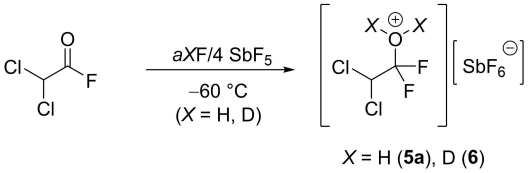

(2)

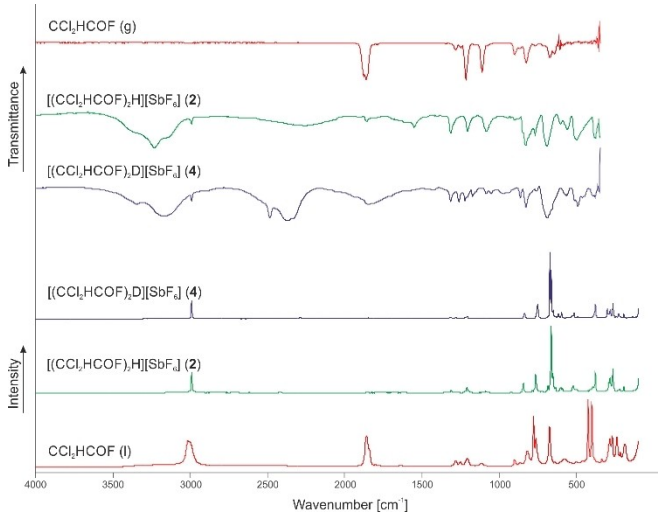

Figure 1. Low-temperature Raman and IR spectra of $[(CCl_2HCOF)_2X][SbF_6]$ (**2**, **4**) (X = H, D) and vibrational spectra of CCl_2HCOF.

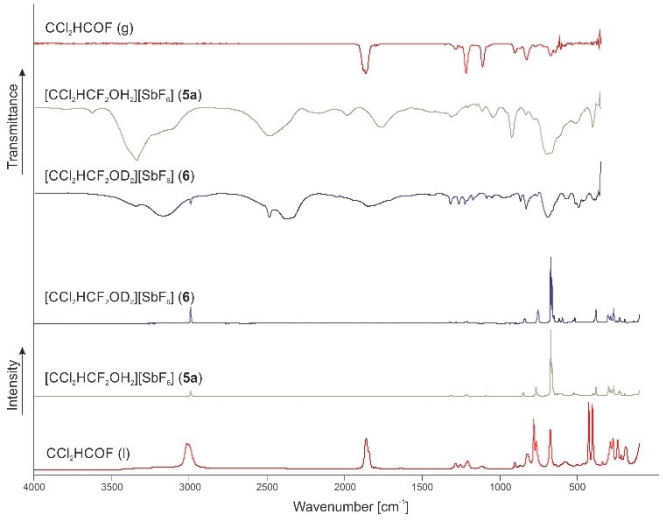

Figure 2. Low-temperature Raman and IR spectra of $[CCl_2HCF_2OX_2][SbF_6]$ (**5a**, **6**) (X = H, D) and vibrational spectra of CCl_2HCOF.

The hexafluoridoarsenates (**1**) and (**3**) decompose at −55 °C, and the hexafluoridoantimonates (**2**) and (**4**) at −40 °C, respectively. **5a** and **6** decompose under the formation of CHF_3, which was confirmed by NMR spectroscopy.

Vibrational Spectroscopy

The low-temperature Raman (Ra) and infrared (IR) spectra of $[(CCl_2HCOF)_2X][SbF_6]$ (**2**, **4**) (X = H, D) and CCl_2HCOF are illustrated in Figure 1, the vibrational spectra of $[CCl_2HCF_2OX_2][SbF_6]$ (**5a**, **6**) (X = H, D) and CCl_2HCOF are depicted in Figure 2. In Table 1 and Table 2 selected observed Raman and IR frequencies of **1**, **2**, **5a**, and **6** are listed together with the quantum chemically calculated frequencies of the cations $[CCl_2HC(OH)F]^+ \cdot CH_2O$ and $[CCl_2HCF_2OH_2]^+ \cdot 2$ HF, which are discussed later. The complete vibrational frequencies of **1**, **2**, **5a**, and **6** as well as their analog *D*-isotopomeric species and the starting material[10] are provided in the Supporting Information (Figures S1-S2 and Tables S1-S3).

Vibrational Spectra of $[(CCl_2HCOF)_2X][AsF_6]$ (1, 3) and $[(CCl_2HCOF)_2X][SbF_6]$ (2, 4) (X = H, D)

For the $[CCl_2HC(OH)F]^+$ cation with C_1 symmetry, 18 fundamental vibrational modes are expected, with all being Raman and IR active. The ν(O–H) is overlaid by condensed water in all IR spectra due to the measuring method. Furthermore, the O–H stretching vibration shows low intensity in the Raman spectra, due to the poor polarizability of the O–H group, which does not apply to the O–D group. The O–D stretching vibration of the *D*-isotopomeric species is observed at 2372 cm^{-1} (**3**) and 2285 cm^{-1} (**4**) in the Raman spectra and at 2363 cm^{-1} in the IR spectrum of **4**. The C=O stretching vibration is detected at 1772 cm^{-1} (Ra) and 1796 cm^{-1} (IR) (**1**) significantly red-shifted by approximately 90 cm^{-1} compared to the starting material. The C–F stretching vibration occurs blue-shifted by around 160 cm^{-1} at 1280 cm^{-1} (**1**) and 1262 cm^{-1} (**2**) (Ra). Furthermore, the ν(C–C) is detected at around 930 cm^{-1} (Ra/IR) at higher frequencies in comparison to the neutral compound. The observed shifts are consistent with the elongation of the C=O

Table 1. Selected experimental vibrational frequencies [cm^{-1}] of $[(CCl_2HCOF)_2H][AsF_6]$ (**1**) and $[(CCl_2HCOF)_2H][SbF_6]$ (**2**) as well as calculated vibrational frequencies [cm^{-1}] of $[CCl_2HC(OH)F]^+ \cdot CH_2O$.

$[(CCl_2HCOF)_2H][AsF_6]$ (**1**)		$[(CCl_2HCOF)_2H][SbF_6]$ (**2**)		$[CCl_2HC(OH)F]^+ \cdot CH_2O$	Assignments		
Raman	IR	Raman	IR	calc.[a,b] (IR/Raman)[c]			
3013(25)	3014 s	2992(32)	2993 m	3019(11/63)	ν_1	A	ν(C–H)
1772(6)	1796 s	1769(2)	1803 w	1707(1499/78)	ν_3	A	ν(C=O)
1281(6)	1286 s	1262(2)		1310(74/2)	ν_5	A	ν(C–F)
928(11)	931 s	925(2)	926 w	910(36/3)	ν_9	A	ν(C–C)
831(21)	833 s	847(15)	833 vs	809(63/4)	ν_{10}	A	ν(C–Cl)
781(66)	779 s	778(6)		767(4/8)	ν_{11}	A	ν(C–Cl)
603(21)	602 s	605(8)	606 m	635(71/2)	ν_{13}	A	ν(C–Cl)

[a] Calculated at the ωB97XD/aug-cc-pVTZ-level of theory. [b] Frequencies are scaled with a factor of 0.956. [c] IR intensity in [km/mol] and Raman intensity in [$Å^4$/u]. Abbreviations for IR intensities: vs = very strong, s = strong, m = medium, w = weak.

Table 2. Selected experimental vibrational frequencies [cm^{-1}] of $[CCl_2HCF_2OH_2][SbF_6]$ (**5a**) and $[CCl_2HCF_2OD_2][SbF_6]$ (**6**) as well as calculated vibrational frequencies [cm^{-1}] of $[CCl_2HCF_2OH_2]^+ \cdot 2$ HF.

$[CCl_2HCF_2OH_2][SbF_6]$ (**5a**)		$[CCl_2HCF_2OD_2][SbF_6]$ (**6**)		$[CCl_2HCF_2OH_2]^+ \cdot 2$ HF	Assignments		
Raman	IR	Raman	IR	calc.[a,b] (IR/Raman)[c]			
2992(10)	2993 w	2992(26)	2991 s	3012(8/71)	ν_1	A′	ν_s(C–H)
1312(2)	1314 m	1313(3)	1315 s	1322(58/1)	ν_{16}	A″	ν_{as}(C–F)
		1283(3)	1262 s	1295(116/4)	ν_4	A′	ν_s(C–F)
		1174(2)	1173 s	1180(103/2)	ν_5	A′	ν_s(C–C)
	1043 m	1055(1)	1053 s	1021(171/1)	ν_6	A′	ν_s(C–O)
846(7)	851 w	838(8)	829 s	820(102/2)	ν_{19}	A″	ν_{as}(C–Cl)
767(14)	771 m	753(22)	762 m	797(219/3)	ν_8	A′	ν_s(C–Cl)

[a] Calculated at the ωB97XD/aug-cc-pVTZ-level of theory. [b] Frequencies are scaled with a factor of 0.956. [c] IR intensity in [km/mol] and Raman intensity in [$Å^4$/u]. Abbreviations for IR intensities: vs = very strong, s = strong, m = medium, w = weak.

bond and the shortening of the C–F as well as the C–C bond, due to hemiprotonation as discussed in the crystallographic section below. The C–Cl stretching vibrations occur at 831 cm^{-1}, 781 cm^{-1}, and 603 cm^{-1} (**1**) (Ra). The C–H stretching and the CCH bending vibrations of the salts (**1**, **2**, **3**, **4**) are not affected by the hemiprotonation.

For the anions $[AsF_6]^-$ and $[SbF_6]^-$, more vibrations are observed than expected for an ideal octahedral symmetry.[11] This is due to distortion in the solid-state and in accordance with the crystal structure.

Vibrational Spectra of $[CCl_2HCF_2OX_2][SbF_6]$ (5a, 6) (X = H, D)

For the $[CCl_2HCF_2OH_2]^+$ cation with C_S symmetry, 24 fundamental vibrational modes are expected, with all being Raman and IR active. The ν_s(O–H) and ν_{as}(O–H) of **5a** are overlaid by condensed water in the IR spectra. The ν_s(O–D) and ν_{as}(O–D) of the *D*-isotopomeric species occur at 2362 cm^{-1} and 2332 cm^{-1} in the IR spectra. The symmetric and antisymmetric C–F stretching vibrations of the CF_2 moiety appear significantly blue-shifted by approximately 200 cm^{-1} at 1312 cm^{-1} (**5a**), 1313 cm^{-1}, and 1283 cm^{-1} (**6**) (Ra) as well as 1314 cm^{-1} (**5a**), 1315 cm^{-1} and 1263 cm^{-1} (**6**) (IR) in comparison to the ν(C–F) of the neutral compound. The ν_s(C–C) of **6** is observed at 1174 cm^{-1} (Ra) and 1173 cm^{-1} (IR). Due to the formation of the oxonium species, the bond is strengthened. Furthermore, the formation of the oxonium species is indicated by the symmetric C–O stretching vibration at 1055 cm^{-1} (**6**) in the Raman spectra and at 1043 cm^{-1} (**5a**) as well as 1053 cm^{-1} (**6**) in the IR spectra. This is consistent with values reported in the literature.[2] The symmetric and antisymmetric C–Cl stretching and CCl_2 bending vibrations of the dichloromethyl group as well as the C–H stretching and CCH bending vibrations of the salts (**5a**, **6**) are not affected by the formation of the oxonium species. For the octahedral anion $[SbF_6]^-$, more vibrations are observed than expected due to interionic interactions leading to a symmetry distortion.[11]

Crystal Structure of $[CCl_2HC(OH)F][(CCl_2HCOF)_2H][SbF_6][Sb_2F_{11}]$

Suitable single-crystals of hemiprotonated dichloroacetyl fluoride were not obtained for measurement. In one case though, single-crystals of **2** melted during the measurement process and recrystallized in the form of a mixed crystal containing the hemiprotonated dichloroacetyl fluoride as well as its fully monoprotonated species. For the latter, there are no indications in the vibrational spectra of the bulk materials **1**, **2**, **3**, or **4**. $[CCl_2HC(OH)F][(CCl_2HCOF)_2H][SbF_6][Sb_2F_{11}]$ crystallizes in the monoclinic space group $P2_1/c$ with two formula units per unit cell. The molecular unit is illustrated in Figure 3. Crystal data and structure refinement are provided in the Supporting Information (Table S4). Selected geometric data are listed in Table 3.

The crystal structure is composed of the hemiprotonated dichloroacetyl fluoride $[(CCl_2HCOF)_2H]^+$ and the monoprotonated species $[CCl_2HC(OH)F]^+$. The bond length C1–O1 (1.209(3) Å) of the hemiprotonated dichloroacetyl fluoride is significantly elongated compared to the starting material (1.190(2) Å)[12] and longer than a formal C=O bond (1.18 Å).[13] The bond C1–F1 (1.299(3) Å) is significantly shortened com-

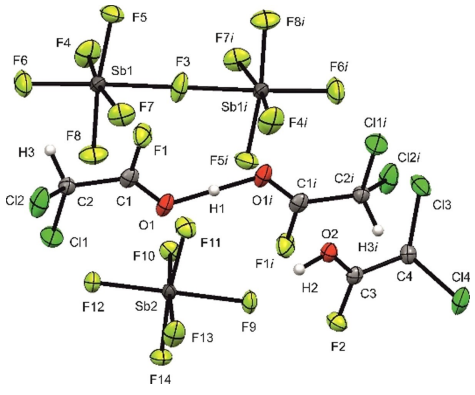

Figure 3. Molecular unit of $[CCl_2HC(OH)F][(CCl_2HCOF)_2H][SbF_6][Sb_2F_{11}]$ (displacement ellipsoids with 50 % probability). Symmetry codes: $i = 1-x, 1-y, 1-z$.

Table 3. Selected bond lengths [Å] and angles [°] of $[CCl_2HC(OH)F][(CCl_2HCOF)_2H][SbF_6][Sb_2F_{11}]$ and donor-acceptor distances. Symmetry codes: $i = 2-x, 1-y, 1-z$.

Bond lengths [Å]			
C1–O1	1.209(3)	C3–O2	1.220(3)
C1–F1	1.299(3)	C3–F2	1.284(3)
C2–C2	1.508(4)	C4–C4	1.498(4)
C2–Cl1	1.736(3)	C4–Cl3	1.745(3)
Bond angles [°]			
Cl1–C2–C1	113.0(2)	Cl3–C4–C3	112.8(2)
C2–C1–O1	126.1(3)	C4–C3–O2	124.1(2)
Dihedral angles [°]			
Cl1–C2–C1–O1	6.3(4)	Cl3–C4–C3–O2	−13.4(4)
Interatomic contacts [Å]			
O2(–H2)···F9	2.394(2)	O1(–H1)···O1*i*	2.449(3)
C3···F10*i*	2.532(3)	C1···F4	2.854(3)
C4···F10*i*	2.876(3)	C1···F7	2.581(3)

pared to the neutral compound (1.336(2) Å).[12] Furthermore, the bonds C1–C2 (1.508(4) Å) as well as C2–Cl1 (1.736(3) Å) are significantly shortened compared to dichloroacetyl fluoride (1.534(4) Å and 1.768(1) Å, respectively).[12] The CCl_2H moiety of the cation displays *gauche* conformation in terms of the carbonyl group with a dihedral angle of 6.3(4)° (Cl1–C2–C1–O1).

For the fully monoprotonated species analog trends are observed. Thus, the bond C3–O2 (1.220(3) Å) is significantly elongated compared to the starting material (1.190(2) Å),[12] but also longer than the C1–O1 bond (1.209(3) Å) of the hemiprotonated species. This is consistent with values of monoprotonated haloacetyl fluorides reported in the literature.[8] Furthermore, the bond length C3–F2 (1.284(3) Å) is shortened compared to the bond C1–F1 (1.299(3) Å) and the bonds C3–C4 (1.498(4) Å) as well as C4–Cl3 (1.745(3) Å) are shortened compared to the bonds C1–C2 (1.508(4) Å) and C2–Cl1 (1.736(3) Å) of the hemiprotonated dichloroacetyl fluoride. The dihedral angle Cl3–C4–C3–O2 is −13.4(4)° and thus, the CCl_2H moiety is arranged in *gauche* conformation with regard to the carbonyl group, as well.

The Sb–F bond lengths of $[SbF_6]^-$ are in the range between 1.858(2) Å and 1.950(2) Å and correspond with values reported in the literature.[14–16] Due to solid-state effects, the anion displays distorted octahedral symmetry. The bonds Sb2–F9 and Sb2–F10 are significantly longer than the other Sb–F bonds because they are involved in hydrogen bonding and C···F interactions. The Sb–F bond lengths of $[Sb_2F_{11}]^-$ are in the range between 1.851(2) Å and 2.0176 Å and are consistent with values reported in the literature.[17–20] The anion displays a linear bond angle Sb1–F3–Sb1*i* (180.0°).[19]

In the crystal structure the fully monoprotonated species is linked to the anion $[SbF_6]^-$ by the strong hydrogen bond O2(–H2)···F9 (2.394(2) Å).[21] Layers are formed by the C···F interactions C3···F10*i* (2.532(3) Å) and C4···F10*i* (2.876(3) Å) (see Figure S3).[22] The hemiprotonated dichloroacetyl fluoride forms a layered structure by the C···F interactions C1···F4 (2.854(3) Å) and C1···F4 (2.581(3) Å) (Figure S4).[22] Each formula unit consists of two dichloroacetyl fluoride molecules bridged by the strong hydrogen bond O1(–H1)···O1*i* (2.449(3) Å).[21] Interatomic distances are listed in Table 3.

Crystal Structure of $[CCl_2HCF_2OH_2][SbF_6]$ (5 a)

$[CCl_2HCF_2OH_2][SbF_6]$ (**5 a**) crystallizes in the monoclinic space group $P2_1/m$ with two formula units per unit cell. The molecular unit of **5 a** is illustrated in Figure 4. Crystal data and structure refinement are provided in the Supporting Information (Table S4). Selected geometric data are listed in Table 4.

Due to the formation of the oxonium ion, the bond length C2–O1 (1.418(3) Å) is significantly elongated compared to dichloroacetyl fluoride (1.190(2) Å)[12] and in the range of a formal C–O bond (1.43 Å).[13] The C2–O1 bond is significantly shorter than the values of oxonium species or protonated alcohols reported in the literature.[2,23,24] The C2–F1 bond (1.325(2) Å) is significantly shortened compared to the starting material (1.336(2) Å).[12]

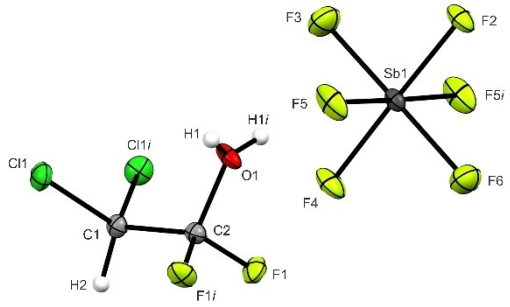

Figure 4. Molecular unit of $[CCl_2HCF_2OH_2][SbF_6]$ (**5 a**) (displacement ellipsoids with 50 % probability). Symmetry codes: $i = x, 0.5-y, z$.

Table 4. Selected bond lengths [Å] and angles [°] of $[CCl_2HCF_2OH_2][SbF_6]$ (**5 a**) and donor-acceptor distances of **5 a**. Symmetry codes: $i = x, 1.5-y, z$; $ii = -x, 0.5+y, -z$; $iii = -x, 1-y, -z$.

Bond lengths [Å]			
C2–O1	1.418(3)	C1–C2	1.528(3)
C2–F1	1.325(2)	C1–Cl1	1.764(1)
Bond angles [°]			
Cl1–C1–C2	108.8(1)	C1–C2–O1	113.7(2)
Dihedral angles [°]			
Cl1–C1–C2–O1	−60.8(1)	Cl1–C1–C2–F1	−179.9(1)
Interatomic contacts [Å]			
O1(–H1)···F5*i*	2.454(1)	F1···F1*iii*	2.653(1)
C1(–H2)···F4*ii*	3.251(3)	Cl1···F6	3.111
O1···F2*ii*	2.708		

The Sb–F bond lengths are in the range between 1.858(2) Å and 1.909(1) Å and are comparable with values reported in the literature.[14–16] Due to solid-state effects, the anion displays distorted octahedral symmetry. The Sb1–F5 bond is significantly longer than other Sb–F bonds, due to hydrogen bonding.

In the crystal structure of **5a**, the ions are arranged into chains along the *a*-axis by the strong hydrogen bond O1(–H1)···F5*i* (2.454(1) Å), the F···F interaction F1···F3*iii* (2.653 Å) and the Cl···F interaction Cl1···F6 (3.111 Å) (Figure 5).[21,22] The ions also form chains along the *c*-axis by the O···F interaction O1···F2*ii* (2.708 Å) and the weak hydrogen bond C1(–H2)···F4*ii* (3.251(3) Å) (see Figure S5).[21,22] All interatomic C···F, O···F, F···F and Cl···F contacts are below the sum of their van der Waals radii (3.17 Å, 2.99 Å, 2.94 Å and 3.22 Å).[22] Interatomic distances are listed in Table 4.

NMR Spectroscopy

Dichloroacetyl fluoride, the hemiprotonated species (**2**), and the oxonium salt (**5a**), respectively, were dissolved in *a*HF, and ^{1}H, ^{19}F, and ^{13}C NMR spectra were measured at −60 °C with acetone-d_6 as external standard. In Table 5, selected observed NMR shifts of the starting material and **5a** are summarized. The measured NMR spectra and the complete NMR data of the neutral compound, **2** and **5a** are listed in the Supporting Information (Figures S6–S11).

In the NMR spectra of the neutral compound, no HF-addition is observed at −60 °C in *a*HF. The NMR spectra of **5a** dissolved in *a*HF display an equilibrium between the oxonium species (**5a**) and the monoprotonated species of dichloroacetyl fluoride (**5b**) in the solution (see Equation 3). Therefore, we assume that in superacidic media the *O*-monoprotonated dichloroacetyl fluoride is formed intermediary and later HF is added to the carbonyl bond to form the oxonium ion. This is discussed in the theoretical section below.

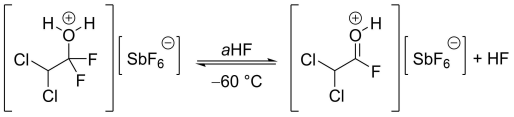

(**5a**) (**5b**) (3)

The ^{1}H NMR spectrum shows a doublet at 5.73 ppm for the CCl_2H moiety of **5b** with a vicinal proton-fluorine coupling constant ($^{3}J_{H–F}$) of 1.7 Hz. This value can be used to get information on the conformation of the cation in solution. The so-called *Karplus equation* describes the correlation of $^{3}J_{H–H}$ or $^{3}J_{H–F}$ coupling constants and dihedral angles in NMR spectroscopy.[25–30] Thus, for angles of 0° and 180°, maximal coupling constants of 30 Hz to 45 Hz are expected, which decrease to a minimum at 90° (~0 Hz).[25–30] Therefore, we assume a dihedral angle near 90° between the C–H and C–F bond of **5b** in solution representing a *gauche* conformation of the CCl_2H moiety in relation to the C=O bond. This was also observed in the crystal structure of **2**.

After measuring the NMR spectra at −60 °C, the sample of **5a** dissolved in *a*HF was warmed up to room temperature to determine the decomposition products of **5a**. Again, ^{1}H and ^{19}F NMR spectra were measured. As shown in Figure S12, **5a** decomposes under the formation of CHF_3.

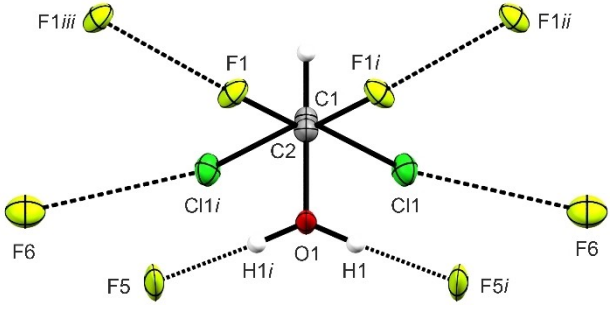

Figure 5. Interatomic contacts along the *a*-axis of $[CCl_2HCF_2OH_2][SbF_6]$ (**5a**) (displacement ellipsoids with 50% probability). Symmetry codes: *i* = *x*, 1.5−*y*, *z*; *ii* = −*x*, 0.5+*y*, −*z*; *iii* = −*x*, 1−*y*, 1−*z*.

Table 5. Selected ^{1}H, ^{19}F, and ^{13}C NMR chemical shifts [ppm] of CCl_2HCOF, $[CCl_2HCF_2OH_2][SbF_6]$ (**5a**), and $[CCl_2HC(OH)F][SbF_6]$ (**5b**) in *a*HF at −60 °C.

	CCl_2HCOF	(**5a**)	(**5b**)
δ ^{1}H obs [ppm]	5.74 (m)	5.38 (t)	5.73 (d)
δ ^{19}F obs [ppm]	20.24 (s)	−81.84 (s)	30.19 (d)
δ ^{13}C obs [ppm]	60.2 (d) (**C**Cl_2H)	64.9 (t) (**C**Cl_2H)	59.3 (d) (**C**Cl_2H)
	158.2 (d) (**C**OF)	119.3 (t) (**C**F_2)	170.8 (d) (**C**(OH)F)

Theoretical Calculations

Quantum chemical calculations were performed at the ωB97XD/aug-cc-pVTZ-level of theory.[31] Solid-state effects and intermolecular interactions as well as hemiprotonation were simulated by respectively adding additional HF and formaldehyde molecules to the cations in the gas-phase.[32] In the Supporting Information (Figures S13–S15), the calculated cations are illustrated with selected bond lengths and angles in comparison to the crystal structures. The calculated values of the complexed cations are in good agreement with the experimentally obtained data.

Mapped Electrostatic Potentials (MEP) were calculated together with Natural Population Analysis (NPA) charges to investigate the HF-addition to the carbonyl bond. Figure 6 depicts the MEP together with the NPAs of $[CCl_2HC(OH)F]^{+}$·HF. In the Supporting Information (see Figure S16 and Table S9), the MEP and the NPAs of dichloroacetyl fluoride are illustrated.

According to the calculations, the positive electrostatic potential (blue) in the neutral compound is located at the two neighboring carbons and the hydrogen, whereas protonation leads to an electron-deficient moiety in the region of the carbonyl carbon, a so-called π-hole.[33–35] This indicates that the positive charge is located at the carbon (see Figure 7). This is

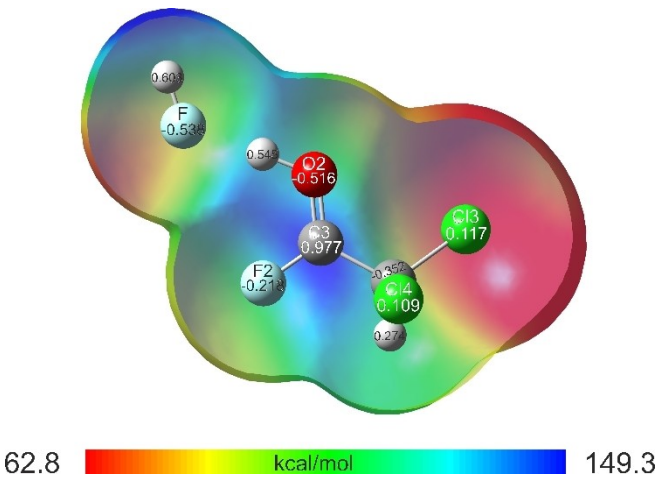

Figure 6. Molecular 0.0004 bohr^{-3} 3D isosurfaces with mapped electrostatic potential as color scale from 62.8 kcal/mol (red) to 149.3 kcal/mol (blue). The electrostatic potential isosurfaces and the NPA charges have been calculated for $[CCl_2HC(OH)F]^+ \cdot HF$.

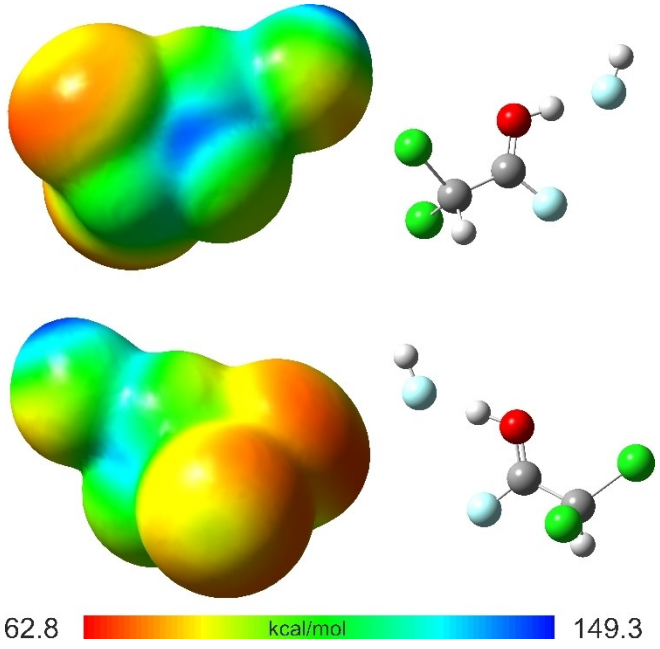

Figure 7. Molecular 0.0004 bohr^{-3} 3D isosurfaces with mapped electrostatic potential as color scale from 62.8 kcal/mol (red) to 149.3 kcal/mol (blue). The electrostatic potential isosurfaces and the NPA charges have been calculated for $[CCl_2HC(OH)F]^+ \cdot HF$. Top: "hydrogen site", bottom: "chlorine site".

confirmed by the NPA charges. The positive charge on the carbonyl carbon increases significantly due to protonation. While the positive electrostatic potential in the neutral compound is distributed over both carbons, the electrophilicity of the carbonyl carbon is not high enough to add HF. Due to protonation, its electrophilicity increases massively. This confirms the experimental results and the presumption that HF-addition occurs after protonation. Interestingly, the π-hole at the carbonyl carbon can only be observed from one side in the MEPs of the HF-complexed cation (Figure 7, top, "hydrogen site"), while the other side is sterically hindered by the large chlorine of the dichloromethyl group (Figure 7, bottom, "chlorine site") because of *gauche* conformation in solution and the solid.

Conclusions

Dichloroacetyl fluoride forms the *O*-hemiprotonated species in the binary superacidic systems HF/MF_5 and DF/MF_5 (M = As, Sb). When SbF_5 is applied in fourfold excess, a tertiary oxonium salt was isolated after HF-addition to the carbonyl bond. The colorless salts were characterized by low-temperature vibrational spectroscopy and the crystal structures of $[CCl_2HC(OH)F][(CCl_2HCOF)_2H][SbF_6][Sb_2F_{11}]$ and $[CCl_2HCF_2OH_2][SbF_6]$ were determined by single-crystal X-ray diffraction analyses. Furthermore, it was demonstrated by low-temperature NMR spectroscopy that the neutral compound shows no HF-addition in *a*HF, whereas an equilibrium between the oxonium species (**5a**) and the monoprotonated dichloroacetyl fluoride (**5b**) exists in solution. The experimental data were discussed together with quantum chemical calculations at the ωB97XD/aug-cc-pVTZ-level of theory. To investigate the HF-addition, Mapped Electrostatic Potentials (MEP) and Natural Population Analysis charges (NPA) of the cations were calculated. Monoprotonation of the carbonyl bond leads to a significant increase of the electrophilicity of the carbonyl carbon, which initiates HF-addition to form an oxonium ion.

Experimental Section

Caution! Avoid skin contact with all compounds. Hydrolysis can lead to formation of HF or DF that burns skin and causes irreparable damage. Ensure appropriate safety precautions while handling with these materials.

Apparatus and Materials: All reactions were performed employing standard Schlenk techniques using a stainless-steel vacuum line. Syntheses were carried out using FEP/PFA tube reactors closed with stainless-steel valves. Prior to the use, the stainless-steel vacuum line and all reactors were dried with fluorine. Low-temperature Raman spectra were recorded under vacuum using glass cells cooled with liquid nitrogen and a Bruker® MultiRamII FT Raman spectrometer equipped with Nd:YAG laser (λ = 1064 nm) and a laser excitation of 500–1000 mW. Low-temperature IR spectra were recorded with a Bruker® Vertex FT IR spectrometer at −196 °C. For measurements, low-temperature IR cells[36] were prepared with CsBr single-crystal plates coated with a small amount of the samples. For visualization, the software Advanced Chemistry Development Inc.® (ACD/Labs 2015) was employed. Low-temperature X-ray diffraction was performed with an Oxford XCalibur3 diffractometer equipped with a Spellman Generator (50 kV, 40 mA) and a Kappa CCD detector, using Mo–Kα radiation (λ = 0.71073 Å). The programs CrysAlisPro 1.171.39.46e (Rigaku OD, 2018)[37] and CrysAlisPro 1.171.40.82a (Rigaku OD, 2020)[38] were employed for the data collection and reduction. The structure solution and refinement were employed with the software SHELXT[39] and SHELXL-2018/3,[40] implemented in the WinGX software package.[41] The solution was checked with the program PLATON[42] and the absorption correc-

tion was performed using the SCALE3 ABSPACK multi-scan-method.[43] Selected data and parameters of the single-crystal X-ray structure analyses are summarized in Table S4 for (**2**) and (**5 a**), respectively (see Supporting Information). Crystallographic data (excluding structure factors) for the structures in this paper were deposited at the Cambridge Crystallograpic Data Centre, CCDC, 12 Union Road, Cambridge CB21EZ, UK. Copies of the data can be obtained free of charge on quoting the depository number CCDC-2068986 for $[CCl_2HC(OH)F][(CCl_2HCOF)_2H][SbF_6][Sb_2F_{11}]$ (**2**) and CCDC-2068988 for $[CCl_2HCF_2OH_2][SbF_6]$ (**5 a**) (Fax: +44-1223-336-033; E-Mail: deposit@ccdc.cam.ac.uk, http://www.ccdc.cam.ac.uk). NMR samples were prepared by transferring the HF solution into a small FEP tube under a nitrogen stream. The tube was sealed under vacuum and inserted into a standard NMR tube. For ^{1}H, ^{19}F and ^{13}C NMR measurements, a JEOL ECX 400 and Bruker BioSpin GmbH AV400RT NMR spectrometer were used with acetone-d_6 as external standard. For evaluation, MNOVA by Mestrelab was used.[44] Quantum chemical calculations were performed on the ωB97XD/aug-cc-pVTZ-level of theory.[31] GaussView 6.0 was used for visualization and illustration of the MEP calculations.[45]

Typical procedure (TP1): Synthesis of *O*-hemiprotonated dichloro-acetyl fluoride and oxonium salts using superacidic systems HF/MF_5 (*M* = As, Sb): The Lewis-acid and anhydrous hydrogen fluoride were condensed into a FEP tube-reactor at −196 °C. To form the superacid, the mixture was warmed to −50 °C, and both components were mixed. After the mixture was cooled to −196 °C again, dichloroacetyl fluoride was condensed into the reaction vessel. Subsequently, the mixture was warmed up to −60 °C, and all components were reacted. Then, the temperature was reduced to −196 °C, again. The remaining HF was removed in a dynamic vacuum at −78 °C. The salts were obtained in quantitative yields as colorless solids.

Synthesis of $[(CCl_2HCOF)_2H][AsF_6]$: Compound (**1**) was prepared from arsenic pentafluoride (2.35 mmol, 399 mg. 4.0 eq.), anhydrous hydrogen fluoride (100 mmol, 2 mL) and dichloroacetyl fluoride (0.880 mmol, 114 mg, 1.0 eq.) as described in TP1. Compound (**3**) was prepared analogously, using *a*DF instead of *a*HF.

Synthesis of $[(CCl_2HCOF)_2H][SbF_6]$: Compound (**2**) was prepared from

antimony pentafluoride (1.25 mmol, 271 mg, 1.0 eq.), anhydrous hydrogen fluoride (100 mmol, 2 mL) and dichloroacetyl fluoride (1.25 mmol, 162 mg, 1.0 eq.) as described in TP1. Compound (**4**) was prepared analogously, using *a*DF instead of *a*HF.

Synthesis of $[CCl_2HCF_2OH_2][SbF_6]$: Compound (**5 a**) was prepared from antimony pentafluoride (2.3 mmol, 0.50 g, 4.0 eq.), anhydrous hydrogen fluoride (50 mmol, 1 mL) and dichloroacetyl fluoride (0.58 mmol, 77 mg, 1.0 eq.) as described in TP1. Compound (**6**) was prepared analogously, using *a*DF instead of *a*HF.

Acknowledgements

We are grateful to the Department of Chemistry of the Ludwig Maximilian University, the Deutsche Forschungsgemeinschaft (DFG), and F-Select GmbH for the financial support of this work. Open Access funding enabled and organized by Projekt DEAL.

Conflict of Interest

The authors declare no conflict of interest.

Data Availability Statement

The data that support the findings of this study are available in the supplementary material of this article.

Keywords: Dichloroacetyl fluoride · superacid · HF-addition · structure elucidation · mapped electrostatic potential

[1] G. A. Olah, G. K. S. Prakash, A. Molnar, J. Sommer, *Superacid Chemistry*, Wiley, Hoboken, New Jersey, **2009**.
[2] R. Minkwitz, S. Reinemann, *Z. Anorg. Allg. Chem.* **1999**, *625*, 121–125.
[3] A. F. Baxter, J. Schaab, J. Hegge, T. Saal, M. Vasilu, D. A. Dixon, R. Haiges, K. O. Christe, *Chem. Eur. J.* **2018**, *24*, 16737–16742.
[4] K. O. Christe, J. Hegge, B. Hoge, R. Haiges, *Angew. Chem. Int. Ed.* **2007**, *46*, 6155–6158.
[5] A. F. Baxter, J. Schaab, K. O. Christe, R. Haiges, *Angew. Chem. Int. Ed.* **2018**, *57*, 8174–8177.
[6] J. Schaab, M. Schwab, D. Kratzert, J. Schwabedissen, H. Stammler, N. W. Mitzel, I. Krossing, *Chem. Commun.* **2018**, *54*, 9294–9297.
[7] S. Andreades, D. C. England, *J. Am. Chem. Soc.* **1961**, *83*, 4670–4671.
[8] S. Steiner, C. Jessen, A. J. Kornath, *Z. Anorg. Allg. Chem.* **2022**, *648*, e202200060.
[9] M. Bayer, C. Kremser, C. Jessen, A. Nitzer, A. J. Kornath, *Chem. Eur. J.* **2022**, *28*, e202104422.
[10] J. R. Durig, M. M. Bergana, H. V. Phan, *J. Raman Spectrosc.* **1991**, *22*, 141–154.
[11] J. Weidlein, U. Müller, K. Dehnicke, *Schwingungsspektroskopie. Eine Einführung*, Thieme, Stuttgart, **1988**.
[12] P. T. Brain, D. W. H. Rankin, H. E. Robertson, M. Bühl, *J. Mol. Struct.* **1996**, *376*, 123–132.
[13] A. F. Holleman, E. Wiberg, N. Wiberg, *Anorganische Chemie*, De Gruyter, Berlin, Boston, **2017**.
[14] R. Minkwitz, N. Hartfeld, C. Hirsch, *Z. Anorg. Allg. Chem.* **1999**, *625*, 1479.
[15] R. Minkwitz, S. Schneider, *Angew. Chem. Int. Ed.* **1999**, *38*, 210.
[16] R. Minkwitz, C. Hirsch, T. Berends, *Eur. J. Inorg. Chem.* **1999**, *1999*, 2249.
[17] E. Bernhardt, B. Bley, R. Wartchow, H. Willner, E. Bill, P. Kuhn, I. H. T. Sham, M. Bodenbinder, R. Bröchler, F. Aubke, *J. Am. Chem. Soc.* **1999**, *121*, 7188–7200.
[18] J. Burgess, C. J. W. Fraser, V. M. McRae, R. D. Peacock, D. R. Russell, *J. Inorg. Nucl. Chem.* **1976**, *28*, 183–188.
[19] I. H. T. Sham, B. O. Patrick, B. Ahsen, S. Ahsen, H. Willner, R. C. Thompson, F. Aubke, *Solid State Sci.* **2002**, *4*, 1457–1463.
[20] M. D. Lind, K. O. Christe, *Inorg. Chem.* **1972**, *11*, 608–612.
[21] G. A. Jeffrey, *An introduction to hydrogen bonding*, Oxford University Press, New York, **1997**.
[22] A. Bondi, *J. Phys. Chem.* **1964**, *68*, 441.
[23] R. Minkwitz, S. Schneider, *Z. Anorg. Allg. Chem.* **1998**, *624*, 1989.
[24] A. Karmakar, L. M. D. R. S. Martins, M. F. C. G. da Silva, S. Hazra, A. J. L. Pombeiro, *Catal. Lett.* **2015**, *145*, 2066.
[25] H. Friebolin, *Ein- und zweidimensionale NMR-Spektroskopie. Eine Einführung*, Wiley-VCH, Weinheim, **2013**.
[26] A. M. Ihrig, S. L. Smith, *J. Am. Chem. Soc.* **1970**, *92*(4), 759–763.
[27] R. J. Abraham, L. Cavalli, K. G. R. Pachler, *Mol. Phys.* **1966**, *11*, 471–494.
[28] K. L. Williamson, Y. F. Hsu, F. H. Hall, S. Swager, *J. Am. Chem. Soc.* **1968**, *90*, 6717–6722.
[29] J. Lambert, J. D. Roberts, *J. Am. Chem. Soc.* **1965**, *87*, 3891–3895.

[30] F. A. Bovey, E. W. Anderson, F. P. Hood, R. L. Kornegay, *J. Chem. Phys.* **1964**, *40*, 3099–3109.
[31] M. J. Frisch, G. W. Trucks, H. B. Schlegel, G. E. Scuseria, M. A. Robb, J. R. Cheeseman, G. Scalmani, V. Barone, B. Mennucci, G. A. Petersson,H. Nakatsuji, M. Caricato, X. Li, H. P. Hratchian, A. F. Izmaylov, J. Bloino, G. Zheng, J. L. Sonnenberg, M. Hada, M. Ehara, K. Toyota, R. Fukuda, J. Hasegawa, M. Ishida, T. Nakajima, Y. Honda, O. Kitao, H. Nakai, T. Vreven, J. A. Montgomery, J. E. Peralta, F. Ogliaro, M. Bearpark, J. J. Heyd, E. Brothers, K. N. Kudin, V. N. Staroverov, R. Kobayashi,J. Normand, K. Raghavachari, A. Rendell, J. C. Burant, S. S. Iyengar,J. Tomasi, M. Cossi, N. Rega, J. M. Millam, M. Klene, J. E. Know, J. B. Cross, V. Bakken, C. Adamo, J. Jaramillo, R. Gomperts, R. E. Stratmann, O. Yazyev, A. J. Austin, R. Cammi, C. Pomelli, J. O. Ochterski, R. L. Martin, K. Morokuma, V. G. Zakrzweski, G. A. Voth, P. Salvador, J. J. Dannenberg, S. Dapprich, A. D. Daniels, O. Farkas, J. B. Foresman, J. V. Ortiz, J. Cioslowski, D. J. Fox, *Gaussian16, Revision C.01*, Gaussian Inc., Wallingford CT, **2016**.
[32] T. Soltner, N. Goetz, A. Kornath, *Eur. J. Inorg. Chem.* **2011**, *20*, 5429–5435.
[33] I. Alkorta, J. Elguero, A. Frontera, *Crystals* **2020**, *10*, 180.
[34] G. Frenking, W. Koch, H. Schwarz, *J. Comput. Chem.* **1986**, *7*, 406–416.
[35] G. A. Olah, G. Liang, Y. K. Mo, *J. Org. Chem.* **1974**, *39*(16), 2394–2398.
[36] L. Bayersdorfer, R. Minkwitz, J. Jander, *Z. Anorg. Allg. Chem.* **1972**, *393*(2), 137–142.
[37] Rigaku Oxford Diffraction, CrysAlisPro Software System, *Version 1.171.39.46e*, Rigaku Corporation, Oxford, UK, **2018**.
[38] Rigaku Oxford Diffraction, CrysAlisPro Software System, *Version 1.171.40.82a*, Rigaku Corporation, Oxford, UK, **2020**.
[39] G. M. Sheldrick, *Acta Crystallogr. Sect. A* **2015**, *71*, 3.
[40] G. M. Sheldrick, *Acta Crystallogr. Sect. C* **2015**, *71*, 3.
[41] L. J. Farrugia, *J. Appl. Crystallogr.* **1999**, *32*, 837–838.
[42] A. Spek, PLATON, *A Multipurpose Crystallographic Tool*, Utrecht University, Utrecht (The Netherlands), **1999**.
[43] *SCALE3 ABSPACK – An Oxford Diffraction Program*, Oxford Diffraction Ltd., UK, **2005**.
[44] *MestReNova 14.0*, Mestrelab Research, **2019**.
[45] R. Dennington, T. A. Keith, J. M. Millam, *GaussView Version 6.0*, Semi-chem Inc. Shawnee Mission, KS, **2016**.

Manuscript received: January 23, 2024
Accepted manuscript online: February 15, 2024